J Porous Mater
DOI 10.1007/s10934-007-9098-2

Thermal and acid treatment on natural raw diatomite influencing in synthesis of sodium zeolites

Kunwadee Rangsriwatananon · Aphiruk Chaisena · Chutima Thongkasam

Received: 25 August 2006 / Revised: 28 December 2006

Abstract A natural raw diatomite and four modified diatomites by calcination and acidification were used as starting materials for the sodium zeolitization process. Iron impurity content present in the natural raw diatomite which was expressed as Fe_2O_3 is about 5.8% and Q^4 ($[Si(OSi)_4]$) unit 64%, whereas the modified diatomite which was treated with hot 6 M H_2SO_4 (refluxed at 100 °C) for 24 h and followed with calcination at 1100 °C for 5 h, contains about 0.5% of Fe_2O_3 and 97% of Q^4. The results showed that under the studied conditions (NaOH 10–30%w/v, 100–180 °C, solid:liquid 1:10 and 1:30, reaction time 24–180 h) only Na-P1, analcime, cancrinite and hydroxysodalite were obtained and the highest yield of each sodium zeolite product was obtained from the modified diatomite treated with hot H_2SO_4 and followed with calcinations at 1100 °C. This results from the reduction of iron content by acid leaching and the elimination of silanol groups after calcination to form more siloxane groups in the structure of starting materials. In addition, a role of iron content was found to be significant in zeolite formation compared to a role of Q^4 sites. It was found that a percentage of crystallinity is very high in the case of all starting materials, which first underwent iron impurity elimination before further thermal treatments.

K. Rangsriwatananon (✉) · C. Thongkasam
School of Chemistry, Institute of Science, Suranaree University of Technology, 111 University Avenue, Nakhon Ratchasima 30000, Thailand
e-mail: kunwadee@sut.ac.th

A. Chaisena
School of Applied Chemistry, Faculty of Science, Lampang Rajabhat University, Lampang, Thailand

Keywords Diatomite · Sodium zeolites · Acid treatment · Thermal treatment · Synthesis

1 Introduction

Zeolites have gained a great deal of attention from many industrial sectors because of their special properties. They have been widely used in many applications, such as ion exchange, adsorbent and catalyst [1]. Therefore, an attempt to search for a zeolite synthesis process with economical value has been regularly of interest. In general, locally obtained raw materials used for silica or alumina source means the advantage of reduction of the operating budget. Useful information on factors affecting the synthesis specifically structure and chemical composition of starting materials to effectively promote the reaction to yield high zeolite crystallinity is necessary for good investment as well. Diatomite is another interesting material because of its relatively low cost, large reserves and its highly reactive amorphous state in silica skeletons which makes it unnecessary to transform an unreactive state into a reactive state with thermal activation like clay minerals [2–4]. Diatomite is natural amorphous silica engendered by the deposition of diatom skeleton. It is formed by closest packing of hydrous SiO_2 spheres and is classified as opal-A mineralogically. Diatomite usually contains other sediments such as clay and fine sand. In Thailand, the Thai Department of Mineral Resources (DMR) found 500,000,000 tons of natural raw diatomite mainly in Lampang Province; containing highly clay minerals and iron oxide. In addition, it is low in silica but high in alumina compared to other countries [5]. Our previous works [6, 7] reported some physico-chemical properties of the natural raw Lampang diatomite and diatomites treated with

heat and acid, as well as the use of these materials for preparing sodium zeolites by hydrothermal alkaline activation under the influence of various conditions. However, the synthesis of zeolite from diatomite depends on a lot of factors and so it is a structurally and chemically complicated problem.

The objective of this work was to investigate the effect of diatomite structure and iron impurity present in the diatomite on synthesis of sodium zeolites by means of preparing a series of modified raw diatomite samples with thermal and acid before using them as starting materials for zeolites synthesis. ^{29}Si magic angle spinning nuclear magnetic resonance (^{29}Si MAS NMR), X-ray diffraction (XRD) and Fourier transform infrared (FT-IR) spectroscopy were used to analyse the structure of diatomite.

2 Experimental

Natural raw diatomite samples collected from the Mae Tha District, Lampang Province, Thailand, were crushed into aggregate-size pieces in roller mills, air-dried, and gently ground to pass through a 63 μm mesh metal sieve. The particles <63 μm in size were used for zeolitization experiments. The researchers selected the best thermal and acid treatment conditions from our previous study [6] to use for the modifying of natural raw diatomite to be the starting materials for synthesizing zeolites. The modified diatomites were obtained as follows: (1) calcined at 900 °C for 5 h, (2) calcined at 1100 °C for 5 h, (3) treated with hot 6 M H_2SO_4 (refluxed at 100 °C) for 24 h and (4) treated with hot 6 M H_2SO_4 (refluxed at 100 °C) for 24 h and followed with calcination at 1100 °C for 5 h. The starting diatomite materials were designated as follows: D-H_2SO_4-C(T), D denoted the natural diatomite, H_2SO_4 denoted the acid treatment with hot 6 M H_2SO_4 and C(T) denoted calcined temperature when T being the calcination temperature. Thus, in this study there were five starting diatomite materials denoted as: D, D-C(900), D-C(1100), D-H_2SO_4 and D-H_2SO_4-C(1100). The structural analysis of starting diatomite materials were determined by ^{29}Si magic-angle spinning nuclear magnetic resonance (^{29}Si MAS NMR, Bruker MSL 300). The samples were spun at a frequency of 4.5 kHz in Bruker double air-bearing probes and recycle delay times of 60 s. X-ray fluorescence (Philips, PW 2404, Magix Pro) was used to determine their chemical compositions by borate fusion technique. The mean particle size distribution was determined by a laser light scattering-based particle sizer (Malven Mastersizer S series instrument). Identification of crystalline samples and investigation of morphology of the samples were determined by XRD and scanning electron microscope, respectively. X-ray diffractograms were recorded by Bruker D5005, with CuK_α radiation, Ni filter, $\lambda = 1.54$ SEM micrographs were performed in a JEOL JSM-6400 scanning electron microscope. The materials were put onto a conductive carbon tape and coated with gold to prevent charging. The framework was also confirmed by FT-IR spectroscopy (Perkin-Elmer Spectrum GX). FT-IR was recorded in the region of 4000–370 cm^{-1} with the KBr pellet technique.

The optimal conditions of each sodium zeolite synthesis from the previous preliminary experiments [7] were selected to be used in the following experiments. All zeolite synthesis procedures were carried out with constant ratio (g cm^{-1}) of solid to liquid 1:10 and $Al(OH)_3$ was used to adjust the Si/Al molar ratio of the modified diatomites with acid (D-H_2SO_4 and D-H_2SO_4-C(1100)) to make the Si/Al ratio to be the same as natural raw diatomite. Zeolite Na-P1 was synthesized using five diatomites mixed with 10% NaOH, and the reaction mixture was carried out in Parr bombs with autogenous pressure of the temperature at 100 °C with reaction 72 h. The other zeolites were synthesized with 10% NaOH for analcime, 20% NaOH for cancrinite and 30% NaOH for hydroxysodalite. These synthesis procedures were the same as above but different in reaction temperatures and reaction times; synthesized analcime under the condition of 140 °C for 72 h, cancrinite of 180 °C for 120 h and hydroxysodalite of 100 °C for 120 h. The experiments were performed in an oven with a controller (±1 °C). Once the activation time was reached, the Parr bomb was quenched in cold water to stop the reaction. The solid product was filtered and washed with deionized water to remove excess alkali until the pH of the filtrate became seven. Then, the sample was dried at 110 °C for 24 h and stored in a desiccator.

3 Results and discussion

The morphology of starting materials was shown in Fig. 1. It showed the dominant *A. granulata* species [8]. The micrograph of the diatomite calcined at 900 °C showed the detail of diatomite structure, still in its original geometry. When calcinated at 1100 °C, the diatomite still showed a sign of its original diatomite structure, but the concave and convex surfaces were almost all gone, and smoother surfaces were formed instead. The SEM micrographs of hot acid activation and the ones of hot acid activation and followed with calcination at 1100 °C both showed the original geometry of the pores to be preserved, but there was collapse of skeleton structure. The mean particle sizes of all the starting materials varied in a range of 8.6–19.8 μm. It was found that the particle size distribution of natural diatomite, calcined diatomite at 900 °C and 1100 °C are 8.6, 17.6 and 19.8 μm, respectively. The

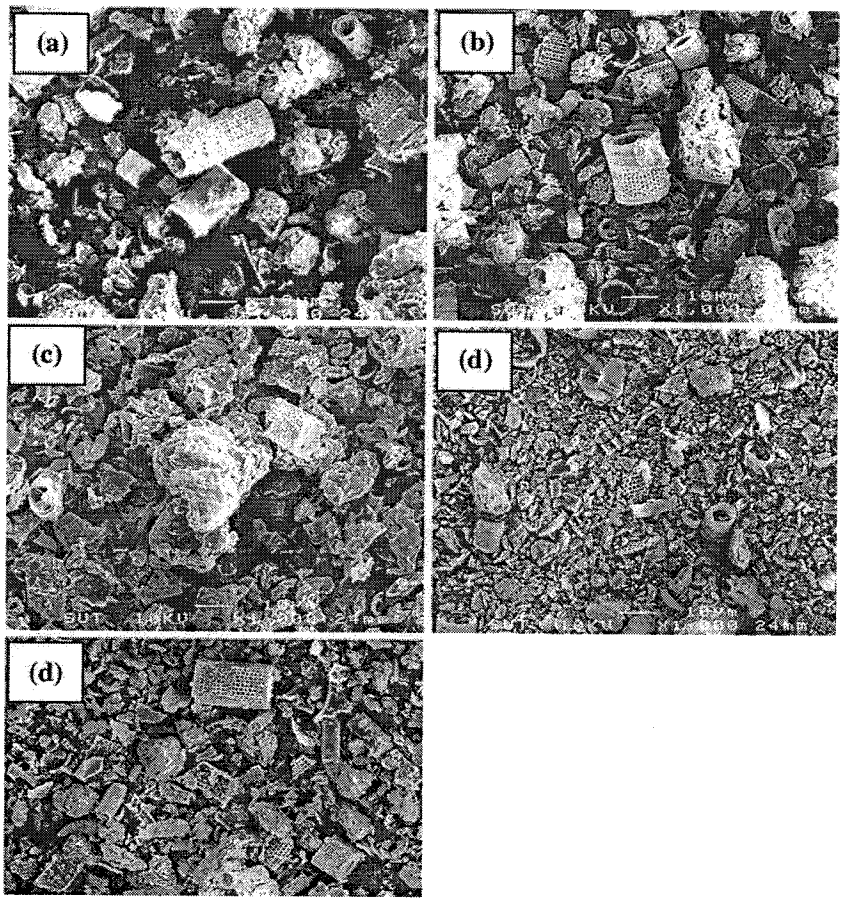

Fig. 1 SEM with 10 kV and 1000 magnification of (**a**) D (**b**) D-C(900) (**c**) D-C(1100) (**d**)D-H_2SO_4 and (**e**) D-H_2SO_4-C(1100), respectively

diatomite treated with hot acid and the one treated with hot acid and followed with calcinations at 1100 °C showed the particle size of 10.8 μm and 9.3 μm, respectively. The elemental composition of the natural raw diatomite and modified diatomite expressed as weight percentages of metal oxide was shown in Table 1. The main components of the natural raw diatomite are oxides of Si, Al and Fe, while the main components of the other samples activated with acid are oxides of Si and Al. The acid treatment reduces or eliminates all other oxides relative to SiO_2. From XRD patterns (see Figs.2–3), the natural diatomite showed

Table 1 The chemical compositions of starting diatomite materials determined by XRF

Diatomite starting material	Chemical content (% weight)							
	SiO_2	Al_2O_3	Fe_2O_3	K_2O	CaO	MgO	MnO	TiO_2
D	71.90	14.60	5.78	1.95	0.17	0.69	0.01	0.51
D-C(900)	76.34	15.43	6.08	1.96	0.17	0.75	0.01	0.53
D-C(1100)	76.73	15.48	6.18	1.92	0.17	0.75	0.01	0.52
D-H_2SO_4	93.56	3.63	0.53	0.80	0.00	0.16	0.00	0.46
D-H_2SO_4-C(1100)	94.42	3.68	0.50	0.68	0.00	0.14	0.00	0.43

a single diffuse band centered at about 23° 2θ which could be identified as biogenic hydrous amorphous silica and also showed quartz at 2θ = 26.6° and 20.9° and some clay minerals like kaolinite, montmorillonite, etc. After calcination at 900 °C, the XRD patterns look similar to raw diatomite whereas calcined diatomite at 1100 °C showed a new peak at 21.8° 2θ as a result from crystalline phase of cristobalite. On the other hand, the sample, with acid before calcining at 1100 °C, could eliminate some impurities, but cristobalite did not appear even at 1100 °C. However, the sample still remained amorphous silica. This suggested that some impurities and/or sufficient amount of Si–OH in the amorphous silica matrix could promote the transformation of some amorphous silica into crystalline structure of cristobalite. It seemed that quartz still remained even when it was treated with hot acid. Our natural raw diatomite sample is yellow powder and becomes white color after acid treatment and becomes red brown color after calcinations. The red brown color appearance corresponds to hematile (α-Fe_2O_3), which exhibited two new peaks at 33.5θ° and 36° 2θ. It is quite difficult from the XRD pattern of the natural raw diatomite sample to indicate what type of compound contributing to its color. However, yellow color of raw diatomite may be obtained

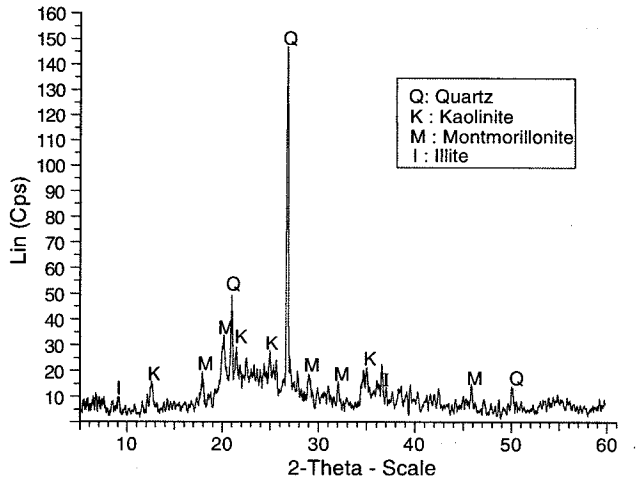

Fig. 2 XRD pattern of the natural raw diatomite compared with the stand pattern from JCPDS database

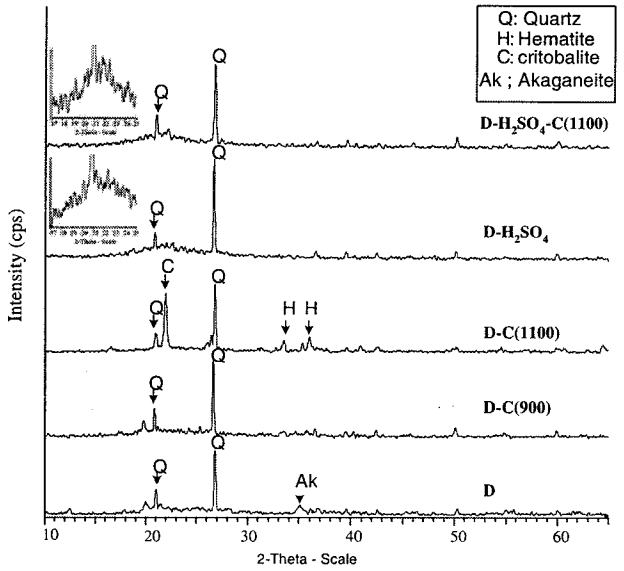

Fig. 3 XRD pattern of starting materials of D, D-C(900), D-C(1100), D-H_2SO_4 and D-H_2SO_4-C(1100), respectively

from goethite (α-FeOOH) as iron impurity, because its pigment is yellow. In addition to this, small broad band appearing at about 35° 2θ may be attributed to akaganeite (β-FeOOH). After calcinations FeOOH may be transformed into α-Fe_2O_3. The analysis of IR spectra shown in Fig. 4. corresponded to the XRD results. The 3698 and 3621 cm^{-1} bands of natural raw diatomite were attributed to OH vibration mode of hydroxyl groups of kaolinite which were eliminated after calcination or acidification [9]. The broad band centered around 3436–3439 cm^{-1} was attributed to OH vibration mode of the physically adsorbed H_2O [10]. The IR band intensities of Si–OH or Al–Al–OH at 913 cm^{-1} and Si–O–Al related to the Al octahedral sheet

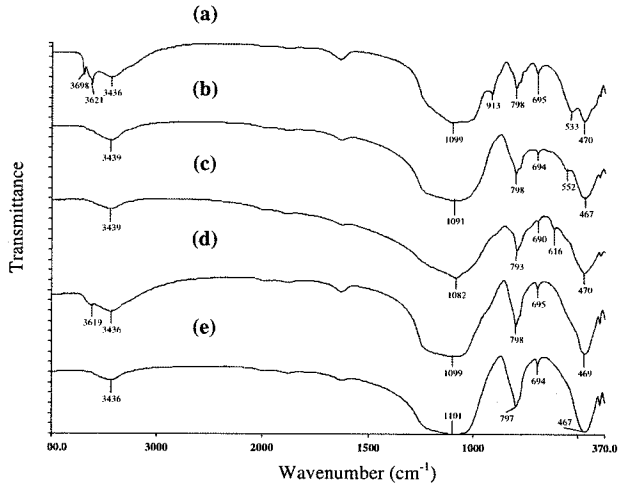

Fig. 4 IR spectra starting materials of (**a**) D (**b**) D-C(900) (**c**) D-C(1100) (**d**)D-H_2SO_4 and (**e**) D-H_2SO_4-C(1100), respectively

found at 533 cm^{-1} was eliminated with hot 6 M H_2SO_4. The result indicates that clay minerals can be removed with hot H_2SO_4. The band around 793–798 cm^{-1} (free silica and/or quartz) is always present in all starting diatomite material and not affected by acid and thermal treatment [11]. The appearance of a new band at 616 cm^{-1} of diatomite calcined at 1100 °C was the typical of critobalite [12]. The absorption bands of diatomite in the region of stretching of vibration of Si–O are quite difficult to solve because of the band interference of clay minerals and types of silica state. However, based on our curve-fitting, the Si–O–T (T = Si or Al) stretch vibrations were assigned at around 1190 cm^{-1}, 1090 $cm^{-1}$and 1030 cm^{-1}. It was found that the relative absorption band area at 1030 cm^{-1} was greatly reduced when natural raw diatomites were treated with heat or acid, whereas the relative band area at 1090 cm^{-1} increased in all modified diatomites. The relative band area at 1190 cm^{-1} for the samples treated with heat was rather similar to the raw diatomite, but increased for the samples treated with acid. This may result from the band at about 1030 cm^{-1}, which was assumed to correspond to the characteristic of clay minerals and/or less active silicate. The band was reduced after acid leaching and transformed after calcinations. After, reactive amorphous silica at about 1090 cm^{-1} and 1190 cm^{-1} was developed. Again, the ^{29}Si MAS NMR technique was used to provide the detailed information on the structure of the starting materials. The ^{29}Si MAS NMR spectra of natural raw diatomite and four modified diatomites were given in Fig. 5. All the spectra were simulated using essentially Gaussian function as illustrated below the spectral traces in Fig. 5. SiO_4 sites were labeled as Q^n, where n designated the number of bridging oxygen atoms (those shared with tetrahedral silicon). The ^{29}Si MAS NMR spectra of all

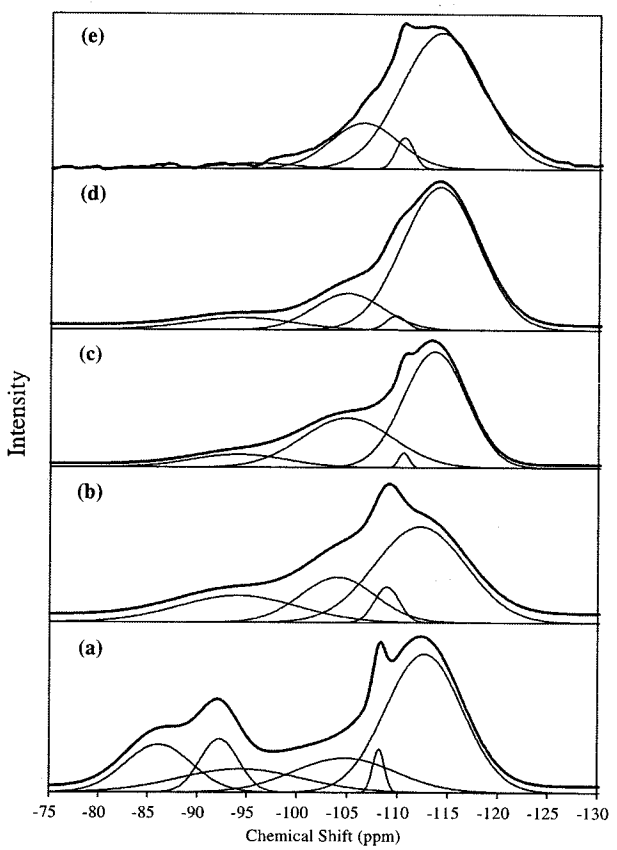

Fig. 5 Experimental and simulated MAS ^{29}Si-NMR spectra (arbitrary Intensity unit) starting materials of (**a**) D (**b**) D-C(900) (**c**) D-C(1100) (**d**)D-H_2SO_4 and (**e**) D-H_2SO_4-C(1100), respectively

samples consisted of four resonances at −95 ± 0.5, −105 ± 1.0, −109.5 ± 1.0 and −113.0 ± 1.0 ppm, except natural raw diatomite having two additional resonances at −86.1 and −92.2 ppm. The characteristic of Q^2 ($[(OH)_2Si(OSi)_2]$) was assigned at −86.1 and −92.2 ppm, Q^3 ($[(OH)Si(OSi)_3]$) at −95 ± 0.5 and Q^4 ($[Si(OSi)_4]$) at, −105 ± 1.0, −109.5 ± 1.0 ppm and 113.0 ± 1.0 ppm [13]. The percentage of Q^n compositions of all starting materials from the fitting were shown in Fig. 6. It showed that Q^2 was eliminated after thermal and acid treatment. The total Q^4 increased continuously after calcination due to dehydroxylation in the order of D, D-C(900), D-C(1100), D-H_2SO_4 and D-H_2SO_4-C(1100). The Q^4 site at around −109 ppm is quite consistent and may be attributed to the crystalline silica phase.

After the hydrothermal process, the received products were identified by comparing the observed powder patterns with calculated ones reported in the collection of simulated XRD patterns for zeolites [14]. The relative intensity yields were obtained from the integrated XRD intensities of the major reflection for each zeolite. The XRD patterns of four series of analcime, cancrinite, Na–P1 and hydroxysodalite obtained from the different starting materials, were shown in Figs. 7–10, respectively. It is clear that under the optimal conditions for synthesizing each zeolite [7], the maximum intensity yield for all zeolites was obtained from the starting material of D-H_2SO_4-C(1100). The pure phase of analcime and cancrinite can be synthesized with almost all starting materials, whereas in the synthesis of Na–P1 and hydroxysodalite, quartz still remained and small amounts of other zeolitic mixed phases appeared. It showed that quartz might not involve in the synthesis under mild condition such as synthesis of Na-P1. To compare the effects of the starting materials to yield the maximum final products, the relative amount of zeolite crystallinity was represented by relative intensity yield (see Fig. 11) which was obtained from integrated XRD intensities of the major reflections with relative intensities more than 50%, such as at 2θ = 12.46°, 17.66°, 21.67°, 28.10° for zeolite Na–P1. In all cases of zeolitization, the relative intensity yields were found to be significantly high in the case of using D-H_2SO_4 and D-H_2SO_4-C(1100) compared to the others (see

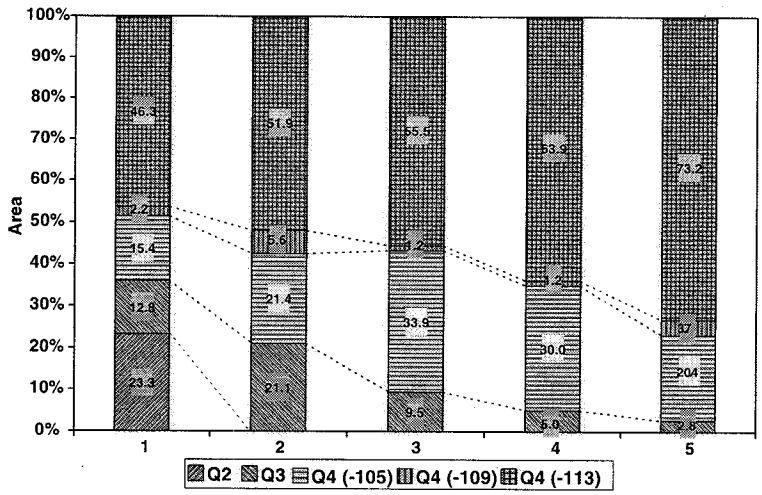

Fig. 6 The percent of Q^2, Q^3, Q^4 from simulation of the ^{29}Si MAS NMR spectra of starting materials; (**1**) D (**2**) D-C(900) (**3**) D-C(1100) (**4**) D-H_2SO_4 and (**5**) D-H_2SO_4-C(1100)

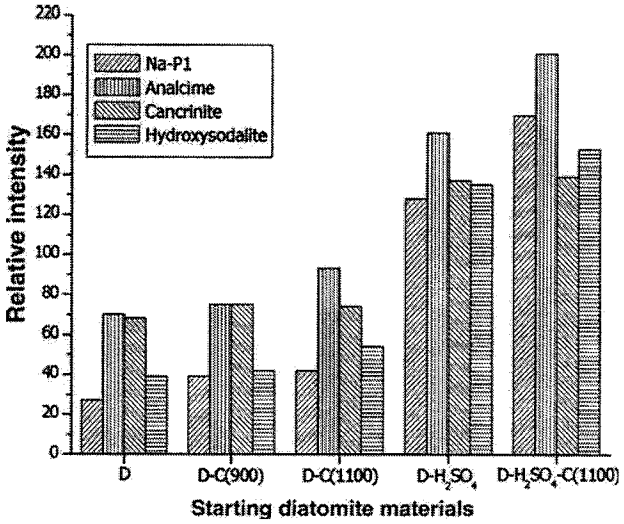

Fig. 11 XRD intensity sodium zeolite yields obtained from the different starting diatomite materials

cinations. Consequently, the relative intensity yields of products obtained from D-C(900), D-C(1100) should be higher than from the natural raw diatomite. However, the present experimental results indicate that amount of iron impurity in natural raw diatomite plays an important role in zeolite synthesis. Amorphous silica containing more Q^4 sites attributes more in zeolitization. Hence, the step of iron elimination in starting raw diatomite is more reasonable to provide high zeolite crystallinity compared to the calcination step.

4 Conclusions

1. Thai natural raw diatomite collected from the main resource in Lampang Province contains quite high amount of iron impurity (about 5.8 wt% expressed as Fe_2O_3) and some clay minerals especially kaolinite.
2. The thermal treatment step gives high amount of Q^4 sites in diatomite structure, depending on the temperature used.
3. Acid treatment can remove iron impurity and some clay minerals from natural raw diatomite and cause the amount of Q^4 sites to increase more than thermal treatment. However, the highest total Q^4 sites are still in the sample treated with hot acid and followed with calcinations at 1100 °C.
4. The crystalline zeolites obtained from the natural raw diatomite and two diatomites treated with heat are much less than from the samples treated with acid. This indicates the influence of iron content on the zeolite formation.
5. The yields from the natural raw diatomite and two calcined diatomites are not much different, even though both of them contain much more amount of the total Q^4 or Q^4 at −113 ppm than the natural raw diatomite, and they also contain some active forms of clay minerals. This indicates that the effect of iron content is significant.
6. In the case of two starting materials from which iron impurity were eliminated first, the highest yields were obtained from the sample after calcining at 1100 °C. It may result from more reactive silica corresponding to Q^4 sites at about −113 ppm. Nevertheless, we suggest that the modification process, eliminating the calcinations step, is more economical.

Acknowledgement This work is supported by Suranaree University of Technology and Lampang Rajabhat University. We are also grateful to Prof. A. Whittaker from The University of Queensland for access to the NMR Spectrometer.

References

1. D.W. Breck, *Zeolite Molecular Sieve.* (John Wiley and Sons, New York, 1974)
2. G. Biswajit, C. Dinesh, B. Subhash, Ind. Eng. Chem. Res. **33**, 2107 (1994)
3. D. Boukadir, N. Bettahar, Z. Derriche, Analyt. Chimica-Sci. Mater. **27**, 1 (2002)
4. V. Sanhueza, U. Kelm, R. Cid, J. Chem. Technol. Biotechnol. **78**, 485 (2003)
5. R. Goren, H. Gocmez, C. Ozgur, Ceram. Int. **32**, 407 (2006)
6. A. Chaisena, K. Rangsriwatananon, Suranaree J. Sci. Technol. **11**, 289 (2004)
7. A. Chaisena, K. Rangsriwatananon, Mater. Lett. **59**, 1474 (2005)
8. R.B. Owen, C. Utha-arron, J. Paleolimnol. **22**, 81 (1999)
9. V.C. Farmer, *Infrared Spectra of Minerals,* Mineralogical Society (London, 1974)
10. P. Yuan, D.Q. Wu, H.P. He, Z.Y. Lin, Appl. Surf. Sci. **227**, 30 (2004)
11. C. Belver, M.A.B. Munoz, M.A. Vicente, Chem. Mater. **14**, 2033 (2002)
12. E. Gorlich, Ceram. Int. **8**, 3 (1982)
13. E. Gunter, Trends Analyt. Chem. **8**, 343 (1989)
14. M.M.A. Treacy, J.B. Higgins, *Collection of Simulated XRD Powder Patterns for Zeolites.* (Elsevier Science Publishers, Amsterdam, 2003)
15. H. Halimaton, N.M.D. Mohd, E. Salasiah, L. Endang, J. Non-Cryst. Solids **211**, 126 (1997)
16. E.I. Basaldella, S.R.M. Torres, J.C. Tara, Clays. Clay. Miner. **5**, 481 (1998)